XXVI. *Further Note on the Propagation of Radio Waves over a Finitely Conducting Spherical Earth.*

By Balth. van der Pol, D.Sc., and H. Bremmer, D.Sc.,
Natuurkundig Laboratorium der N. V. Philips' Gloeilampenfabrieken,
Eindhoven, Holland *.

[Received November 8, 1938.]

Summary.

In a former article (III.) it was pointed out that in the theory of the propagation of radio waves over a finitely conducting earth two different approximations for the many *Bessel* functions occurring in the problem can be introduced, viz., (*a*) the more simple *tang.* approximation (up till now used by most workers in this field), and (*b*) the less simple *Hankel* approximation, but which is required when the wave-length is small compared with the circumference of the earth. In III. the field on the surface of the earth due to an emitter on the ground was calculated with an exclusive use of this better *Hankel* approximation, whereas in II., the superiority of the approximation not being fully realized yet at the time, curves for the field above the ground were calculated with the aid of both approximations. The results obtained there have now been fully recalculated with the exclusive use of the *Hankel* approximation resulting in the figs. 5 and 6, which therefore should replace the former figs. 19 and 20 of II. In these new figures the curves could be given ranging from the immediate proximity of the emitter up to well into the shadow region, due to the good fit existing in the transition region between the geometric optical formula (5) and the residue formula (4 *b*). Here the formerly introduced " divergence factor " was numerically of great importance.

§1. *Introduction.*

In three former papers I., II., and III. † we developed the theory of the propagation of radio waves round a spherical finitely conducting earth. Two different ways of attack were worked out :—

(A) An extension of a series solution first given by G. N. Watson, which is best applicable in the " shadow region " of the emitter and which, further, will be called the Residue-method, and

* Communicated by the Authors.

† Phil. Mag. xxiv. p. 141 (1937) ; xxiv. p. 825 (1937) ; xxv. p. 817 (1938).

(B) an approximate geometric-optical ray expression obtained from the rigorous solution of the problem, which was best applicable in the lit region, and which will, further, be called the geometric-optical method.

In III. we stressed the point that two different approximations to the Bessel functions occurring in the solution (A) could be made use of, viz., what we called (*a*) the *tang.* approximation (I. (16) and III. (10 *a*)), and (*b*) the *Hankel* approximation (I. (17), and III. (10 *b*)), of which, as pointed out in III., the latter is decidedly better for the practical condition $(k_1 a)^{2/3} \gg 1$, although the *tang.* approximation leads to a simpler treatment of the problem. We here use the same notations as in these former papers.

In III. (figs. 3, 4, 5, and 6) we gave a complete set of practical curves for the field on the surface of the earth ($h_2 = 0$) and when the emitter is also on the ground ($h_1 = 0$). These data were all calculated with the aid of the *Hankel* approximation only and therefore constitute a very accurate result.

As to the numerical results for an elevated emitter and (or) receiver (II., figs. 19 and 20), these were obtained partly still with the less accurate *tang.* approximation, the superiority of the *Hankel* approximation not being known yet at the time. We therefore have repeated these numerical investigations for the case of either or both the emitter and receiver at a height of $h = 100$ metres and for $\sigma = 10^{-13}$, $\epsilon = 4$, but now with the exclusive use of the *Hankel* approximation. Moreover, we have taken the opportunity to apply our former geometric-optical solution (B) also numerically, and have obtained an excellent fit between the numerical results calculated according to the methods (A) and (B), so that we could considerably both extend and improve our former data II., figs. 19 and 20, which are therefore to be replaced by the present figures 5 and 6.

In our former investigations we could show that, contrary to the general belief, the waves bend smoothly over the horizon and have still a considerable amplitude in the "shadow region." The present extension of our former investigations fully confims this conclusion, and waves of the order of one centimetre are beyond the horizon even stronger than we thought before. The present investigation also fully confirms our former conclusion that a full cut-off at the horizon only occurs for waves of the order of one millimetre and shorter.

§ 2. *Recapitulation of Former Results.*

We showed that, as a consequence of the strong absorption in the earth, the total field Π_{tot} (even behind the horizon) could be approximated to by the direct radiation $I^e_{-1,0}$ and the once reflected radiation $O^e_{-1,0}$, where

it must be remembered that both these radiations penetrate by diffraction into the " shadow region." This leads in case (A) to the series II. (77), viz. :—

$$\Pi_{\text{tot.}} \sim \mathrm{I}^{e}_{-1,\,0} + \mathrm{O}^{e}_{-1,\,0} = \frac{4\pi i}{(k_1 a)^3} \sum_{s=0}^{\infty} \frac{n_s \cdot e^{i n_s \pi}}{\left(\dfrac{\partial \mathrm{M}_{n-1/2}}{\partial n}\right)_{n=n_s}} \cdot f_s(h_1) \cdot f_s(h_2) \cdot \mathrm{P}_{n_s - 1/2}\{\cos(\pi - \vartheta)\}, \quad (1)$$

where (see II., (76)) the position of the orders n_s is determined by

$$\mathrm{M}_n = \left[\frac{1}{x} \cdot \frac{d}{dx} \log\{x\zeta_n^{(1)}(x)\}\right]_{x=k_1 a} - \left[\frac{1}{x} \cdot \frac{d}{dx} \log\{x\zeta_n^{(2)}(x)\}\right]_{x=k_2 a} = 0 \; . \quad (2)$$

The factors

$$\left.\begin{aligned} f_s(h_1) &= \frac{\zeta^{(1)}_{n_s - 1/2}(k_1 b)}{\zeta^{(1)}_{n_s - 1/2}(k_1 a)} \\ f_s(h_2) &= \frac{\zeta^{(1)}_{n_s - 1/2}(k_1 r)}{\zeta^{(1)}_{n_s - 1/2}(k_1 a)} \end{aligned}\right\} \quad . \; . \; . \; . \; . \; . \; . \; . \quad (3)$$

occurring in (1) may be called the height gain factors, which can be used to extend our formula III. (20 *b*) (which was meant for $h_1 = h_2 = 0$) to

$$\Pi_{\text{tot}} \sim 2 \frac{e^{\frac{1}{8} i k_1 a \vartheta}}{i k_1 a \vartheta} \cdot \sqrt{2\pi i \chi} \cdot \sum_{s=0}^{\infty} f_s(h_1) \cdot f_s(h_2) \cdot \frac{e^{i \tau_s \chi}}{\left(2\tau_s - \dfrac{1}{\delta^2}\right)}, \; . \; . \quad (4\,b)$$

which expression therefore constitutes our present basis as regards the method (A).

On the other hand, the application of the geometric-optical treatment (B) (see II. (91)) leads to

$$\Pi_{\text{tot}} \sim \frac{e^{i k_1 \mathrm{D}}}{i k_1 \mathrm{D}} + \alpha_{11} \cdot \mathrm{R}_{11} \cdot \frac{e^{i k_1 (\mathrm{R}_1 + \mathrm{R}_2)}}{i k_1 (\mathrm{R}_1 + \mathrm{R}_2)}, \; . \; . \; . \; . \; . \quad (5)$$

being the sum of the incident ray and the reflected ray, the amplitude of the latter being given by the product of the " divergence factor " α_{11} and the " spherical reflexion coefficient " R_{11}.

§ 3. *The Height-gain Factors* $f_s(h_1)$ and $f_s(h_2)$.

In II. these factors f_s were only explicitly given in the cases $\delta = 0$ and $\delta = \infty$ where

$$\delta = \frac{i k_2^2 / k_1^2}{(k_1 a)^{1/3} \sqrt{k_2^2/k_1^2 - 1}}.$$

In the general case the *tang.* approximation leads to

$$f_s(h_1)\sim\frac{(-1)^s\sqrt{1-2\tau_s\delta^2}}{\delta\sqrt[4]{-2\tau_s(\chi_1^2-2\tau_s)}}\cdot\cos\left\{\frac{\pi}{4}+\frac{1}{3}(\chi_1^2-2\tau_s)^{3/2}\right\}$$

$$\sim\frac{(-1)\sqrt{1-2\tau_s\delta^2}}{2\delta\sqrt[4]{-2\tau_s(\chi_1^2-2\tau_s)}}e^{i\pi/4+i/3(\chi_1^2-2\tau_s)^{3/2}}, \quad \ldots\ldots (6a)$$

where $$\chi_1=(k_1a)^{1/3}\cdot\sqrt{\frac{2h_1}{a}},$$

and $$\chi_2=(k_1a)^{1/3}\cdot\sqrt{\frac{2h_2}{a}},$$

and a similar expression for $f(h_2)$. As explained above, in II. a combined use was made of the *tang.* and the, better, *Hankel* approximation, but, due to a resonance effect, instead of an improvement, a less accurate result was obtained, which caused in II. (99), (101), and (102) wrong factors to occur. In fact, $\sqrt{\chi_1}$ and $\sqrt{\chi_2}$ are to be replaced by $\sqrt[4]{\chi_1^2-2\tau_s}$, resp. $\sqrt[4]{\chi_2^2-2\tau_s}$, and in the factors $1-\frac{96}{5}\delta\tau_s{}'^2$ the term 1 must be omitted*. Thus if we limit ourselves for the moment to the *tang.* approximation only we obtain for $h_1\neq0$ and $h_2=0$ instead of (101):

$$\Pi_{\text{tot}}\sim\frac{e^{ik_1a\vartheta}}{ik_1a\vartheta}\cdot\sqrt{2\pi\chi}\delta e^{-i\pi/4}\cdot\sum\frac{(-1)^s e^{i\tau_s\chi+i/3(\chi_1^2-2\tau_s)^{3/2}}}{\sqrt[4]{2\tau_s(\chi_1^2-2\tau_s)}\cdot\sqrt{1-2\delta^2\tau}} \quad . \quad (7a)$$

and for both h_1 and h_2 finite instead of (102)

$$\Pi_{\text{tot}}\sim2\frac{e^{ik_1a\vartheta}}{ik_1a\vartheta}\cdot\frac{\sqrt{\pi i\chi}}{4}\cdot\sum\frac{(1-2\delta^2\tau_s)}{\left(1+\frac{\delta}{2\tau_s}-2\delta^2\tau_s\right)}$$

$$\cdot\frac{e^{i\tau_s\chi+i/3(\chi_1^2-2\tau_s)^{3/2}+i/3(\chi_2^2-2\tau_s)^{3/2}}}{\sqrt{\tau}\sqrt[4]{(\chi_1^2-2\tau^s)(\chi_2^2-2\tau_s)}}, \quad \ldots\ldots (8a)$$

both being valid for χ_1^2 and $\chi_2^2\gg3$ and where the former first factor $2e^{ik_1D}/(ik_1D)$ has been replaced by the slightly more accurate expression $2e^{ik_1a\vartheta}/(ik_1a\vartheta)$.

But, as said before, we consider the *Hankel* approximation as the better one of the two, and with it we obtain from II. (97) for $f_s(h_1)$:

$$f_s(h_1)\sim i\sqrt{\frac{\chi_1^2-2\tau_s}{2\tau_s}}\cdot\frac{H^{(1)}_{1/3}\{1/3(\chi_1^2-2\tau_s)^{3/2}\}}{H^{(1)}_{1/3}\{1/3(-2\tau_s)^{3/2}\}}. \quad \ldots\ldots (6b)$$

As (see II., pp. 852 and 853) the $H_{1/3}$ of the nominator of (6 *b*) behaves differently when the argument is $>$ or <1, *i. e.*, when $h_{\text{metre}}>$ or $<56\lambda^{2/3}$,

* Mr. G. Millington, in a private communication, kindly drew our attention to this discrepancy.

we approximate these two cases separately. When $h > 56\lambda^{2/3}$ and for the case of ultra short waves, where $|\delta| \ll 1$, (6 *b*) can further be simplified to

$$f_s(h_1) = \frac{3}{4}\sqrt{\frac{2}{\pi}} \cdot \frac{e^{-i\pi/4+i/3(\chi_1^2-2\tau_s)^{3/2}}}{\delta\tau_{s,0}\sqrt[4]{\chi_1^2-2\tau_s}\cdot[J'_{1/3}(1/3\,|\,2\tau_{s,0}\,|^{3/2})+J'_{-1/3}(1/3\,|\,2\tau_{s,0}\,|^{3/2})]'} \quad . \; . \; . \; . \quad (9\,b)$$

where, for $s \geqslant 4$, the sum $J'_{1/3}+J'_{-1/3}$ may be approximated by

$$\frac{(-1)^{s+1}\sqrt{6}}{\pi\sqrt{s+3/4}}.$$

This formula (9 *b*) was derived from (6 *b*) by replacing $H_{1/3}$ in the nominator by the first term of its asymptotic development, whereas in the denominator $H_{1/3}$ was first expressed in $J_{1/3}$ and $J_{-1/3}$, and thereupon the first two terms of its Taylor development in δ were retained. For h near $56\lambda^{2/3}$ more terms of the asymptotic development of $H_{1/3}$ are necessary.

On the other hand, when $h < 56\lambda^{2/3}$ we better go back to the original definition (3) of $f_s(h)$ which, making use of its differential equation (I. (19)) and of the above equation (2) for the zero's n_s, together with the approximation

$$\left[\frac{d}{dx}\log\{x\zeta_n^{(2)}(x)\}\right]_{x=k_2a} = \frac{k_2}{k_1}\cdot\frac{1}{z^{1/3}\delta},$$

yields

$$f_s(h_1) \sim 1+\left(1-\frac{\delta}{z^{2/3}}\right)\frac{k_1h_1}{z^{1/3}\delta}-(1-z^{2/3}\delta\tau_s)\frac{k_1^2h_1^2}{z^{4/3}\delta} \; \ldots, \; . \; . \quad (10)$$

being a simpler form for II. (98). Moreover, a further consideration shows that (10) leads to a minimum in the field as a function of height, which, for negligible displacement current, occurs at

$$h_{\min} = \frac{\sqrt{c}}{2\pi}\cdot\sigma_{\text{e.m.u.}}^{1/2}\lambda^{3/2},$$

confirming in a simple way a result of Eckersley and Millington *.

The height-gain factors $f_s(h_1)$ and $f_s(h_2)$, appearing in (4 *b*) and which belong to the Residue method (A), have thus been developed in a form suitable for numerical application. In the following paragraphs we shall consider in more detail the *divergence factor* α_{11} and the *spherical reflexion coefficient* R_{11}, both belonging to the geometric-optical approximation (B).

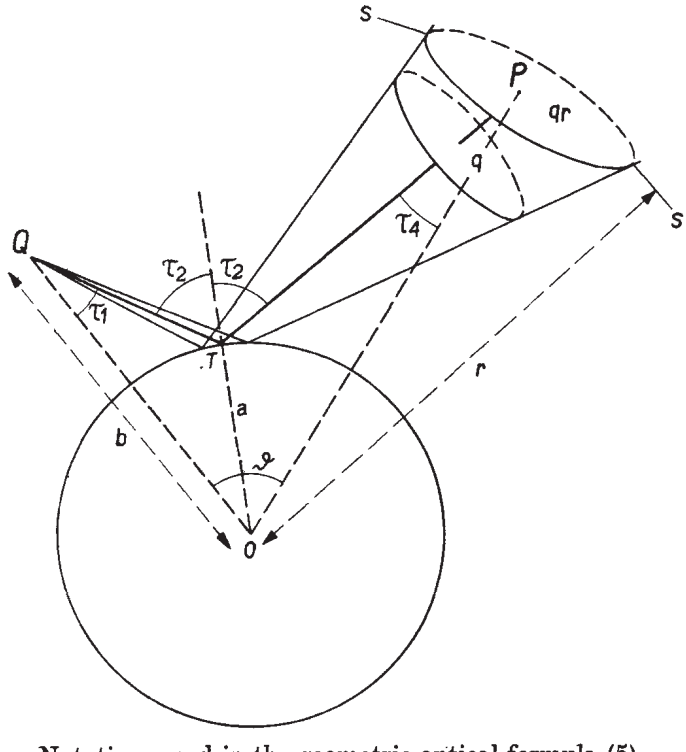
* Phil. Trans. Roy. Soc. ccxxxvii. p. 297 (1938).

§ 4. *The Divergence Factor* α_{11}.

The divergence factor α_{11} was developed in II. (91) from the general wave solution with the aid of the saddle-point method. It was explained physically as the additional divergence of a beam of rays due to the reflexion against a curved surface. The analytical expression found for this geometrical function was

$$\alpha_{11}=\frac{(R_1+R_2)\sqrt{k_1 a \sin\tau_2}}{k_1 br\sqrt{\sin\vartheta\,.\,\frac{\partial\vartheta}{\partial n}\,.\cos\tau_1\cos\tau_4}}=\frac{a(R_1+R_2)\sqrt{\sin\tau_2\cos\tau_2}}{\sqrt{br\sin\vartheta(R_1 r\cos\tau_4+R_2 b\cos\tau_1)}}\,, \quad . \ . \ . \ . \ (11)$$

Fig. 1.



Notations used in the geometric-optical formula (5).

but as this factor is of great numerical importance in determining the field before the horizon we give here another, this time purely geometrical, interpretation of this function.

Consider fig. 1, a narrow beam leaving the source Q and thereupon, after reflexion against the sphere at T, arriving at P. Let q be the actual normal cross-section of this beam at P, and let q' be the cross-section if the

reflexion had taken place against a plane surface at T, then we shall show that

$$\alpha_{11}=\sqrt{\frac{q'}{q}} \quad . \quad . \quad . \quad . \quad . \quad . \quad . \quad . \quad . \quad . \quad (12)$$

Obviously the cross-section q' at P is given by

$$q'=(R_1+R_2)^2.\sin\tau_1.d\tau_1 d\phi,$$

where the angle τ_1 is as shown in fig. 1. The spatial angle of the beam on leaving Q is $\sin\tau_1\, d\tau_1\, d\phi$, where ϕ is measured at right angles to the plane of the paper. The cross-section q_r, which the beam at P cuts out from a sphere S of radius $r=OP$ and centre at O, is

$$q_r=r^2.\sin\vartheta.d\vartheta d\phi.$$

Now, for fixed r, $d\vartheta=\frac{\partial\vartheta}{\partial n}.dn$ (see for definition of $\frac{\partial\vartheta}{\partial n}$ II. p. 843) where $n=k_1 b\sin\tau_1$. Further, we have $dn=k_1 b\cos\tau_1.d\tau_1$, from which it follows that

$$q_r=k_1 b r^2.\sin\vartheta.\frac{\partial\vartheta}{\partial n}.\cos\tau_1.d\tau_1\, d\phi,$$

and also

$$q=q_r.\cos\tau_1.$$

Having thus found q' and q equation (12) at once gives α_{11}, which is therefore seen to be identical with (11). Hence the divergence factor formerly derived with the aid of the saddle-point method can thus be fully explained geometrically.

As to the numerical value of α_{11} this is unity on the lit part of the surface of the sphere, but it becomes zero on the line of sight and elsewhere varies between these two limits.

§ 5. *The Spherical Reflexion Coefficient* R_{11}.

As shown in (5), a numerical knowledge of the spherical reflexion coefficient R_{11} is necessary in order to calculate the field in the lit part of space. The expression for R_{11} found in II. (68 *a*) was

$$R_{11}=\frac{-\left[\frac{1}{x}.\frac{d}{dx}\log\{x\zeta_n^{(2)}(x)\}\right]_{x=k_1a}+\left[\frac{1}{x}.\frac{d}{dx}\log\{x\zeta_n^{(2)}(x)\}\right|_{x=k_2a}}{\left[\frac{1}{x}.\frac{d}{dx}\log\{x\zeta_n^{(1)}(x)\}\right]_{x=k_1a}-\left[\frac{1}{x}.\frac{d}{dx}\log\{x\zeta_n^{(2)}(x)\}\right]_{x=k_2a}} \quad . \quad (13)$$

For a practical case, where the position of the emitter and receiver are given, first the position of the reflexion point T (fig. 1) on the surface of the earth has to be determined, so that then, also, the angle τ_2 is known. Hence in (13) we must take $n=k_1 a\sin\tau_2$, which can be written $n=a\lambda$, where $\lambda=k_1\sin\tau_2$. Our next task is to obtain approximations of the

ζ functions in (13). As further in the $\zeta_n^{(2)}(k_2a)$ functions the argument k_2a is never near the order $n=k_1a\sin\tau_2$, we have, as in I., p. 152,

$$\left[\frac{d}{dx}\log\{x\zeta_n^{(2)}(x)\}\right]_{x=k_1a}\sim\frac{\sqrt{\lambda^2-k_2^2}}{k_2},$$

whereas for the other ζ functions, where the argument k_1a may be near the order $k_1a\sin\tau_2$, we must use the *Hankel* approximation according to I. (22). We thus obtain, instead of (13),

$$R_{11}=\frac{k_2^2\sqrt{\lambda^2-k_1^2}\left[1-\frac{k_1^2}{\lambda^2}\left\{1-e^{-i\pi/6}\cdot\frac{H_{2/3}^{(2)}(u)}{H_{1/3}^{(2)}(u)}\right\}\right]-k_1^2\sqrt{\lambda^2-k_2^2}}{k_2^2\sqrt{\lambda^2-k_1^2}\left[1-\frac{k_1^2}{\lambda^2}\left\{1-e^{i\pi/6}\cdot\frac{H_{2/3}^{(1)}(u)}{H_{1/3}^{(1)}(u)}\right\}\right]+k_1^2\sqrt{\lambda^2-k_2^2}},\qquad(14)$$

where $$u=\frac{a}{3\lambda^2}\cdot(\lambda^2-k_1^2)^{3/2}\cdot e^{3/2i\pi}.$$

Two special cases are of interest :—

(*a*) $a\to\infty$, leading to the plane problem. Here (14) gives at once the well-known Fresnel reflexion coefficient in the form as already considered in I. (21).

(*b*) $\tau_2=\pi/2$ corresponding to grazing incidence. Here $\lambda=k_1$, and hence $u=0$ leading to the special case

$$R_{11}\sim\frac{1-e^{-2/3i\pi}A\delta}{-1+e^{2/3i\pi}A\delta},\qquad(15)$$

where $$A=\frac{6^{1/3}}{2}\cdot\frac{\Pi(2/3)}{\Pi(1/3)}=0{\cdot}919.$$

As for the ultra-short waves and average soil $|\delta|\ll1$, we see from (15) that even for grazing incidence the spherical reflexion coefficient is very approximately equal to -1, which is also the value of the plane reflexion coefficient.

The difference between the spherical and plane reflexion coefficient even at grazing incidence thus being very small, we may, for the conditions mentioned, everywhere in (5) replace the spherical by the ordinary plane reflexion coefficient. This, however, would not be allowed if longer waves or a reflexion against soil of a better conductivity were investigated. *E. g.*, if the conductivity were infinite, ($\delta\to\infty$), (15) would give for the value of the spherical reflexion coefficient at grazing incidence $e^{-i\pi/3}$ instead of $+1$ as for the plane case.

§ 6. *Numerical Results.*

Above we have given all the details for a numerical evaluation of cases of practical importance, all deductions now being exclusively based on the more accurate *Hankel* approximation.

With the aid thereof we have again with great care constructed two sets of curves giving the attenuation (as compared with the free radiation) of the waves as a function of distance, viz. :

(*a*) for $h_1=100$ metres, $h_2=100$ metres,

(*b*) for $h_1=100$ metres, $h_2=0$,

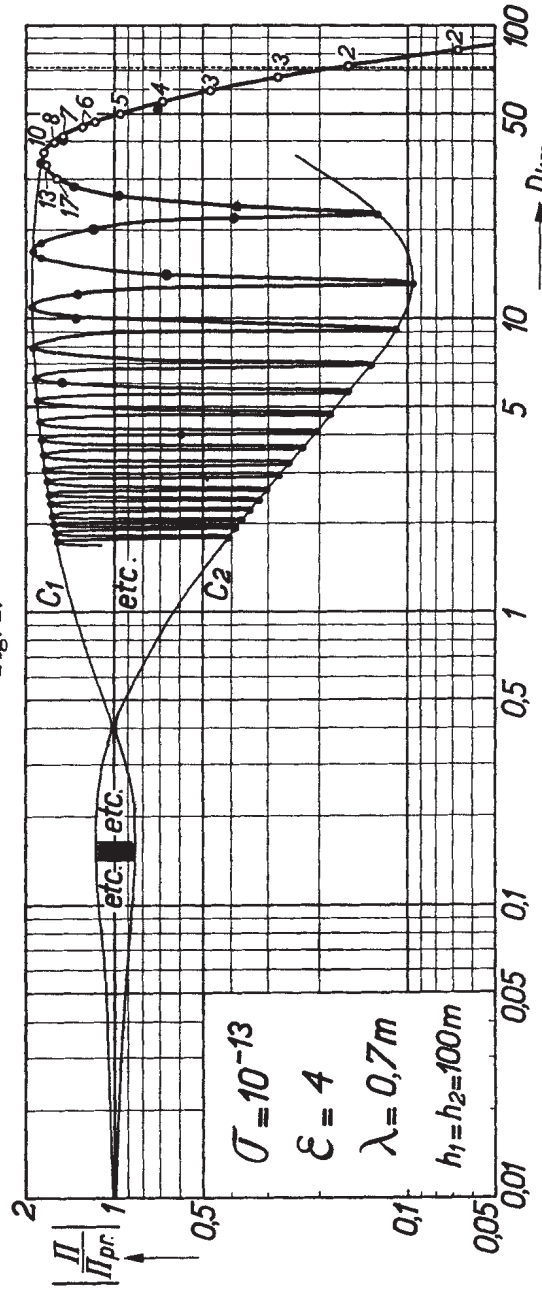
the conductivity σ and dielectric constant ϵ being taken $\sigma=10^{1-3}$ e.m.u., $\epsilon=4$ representing average soil. The range of distance covered is from 0 to well into the "shadow region"; the curves have been calculated for the wave-lengths $\lambda=7$ m., 70 cm., 7 cm., and 7 mm.

As already stated above, the parts of the curves for the lit region were calculated with the geometric-optical formula (5), the divergence factor α_{11} being duly taken into account. On the other hand, the residue formula (4 *b*), which is principally applicable anywhere, is most suited beyond and near the horizon, and a range of overlap with (5) exists, showing a very good numerical agreement. Thus (4 *b*) and (5) together enable us to draw uninterrupted field curves for distances ranging from close to the emitter up to far into the shadow region.

Before, however, describing the final curves we give three additional figures 2, 3, and 4, which show some detailed results of the calculation. Consider first fig. 2, which has been drawn for $\sigma=10^{-13}$, $\epsilon=4$, $\lambda=0{\cdot}7$ metre, $h_1=h_2=100$ metres. In this figure, therefore, the emitter is at a height of 100 metres, whereas the receiver is thought to be all the time at the same height, the linear distance D being varied. Up to the shadow limit maxima and minima occur due to the interference of the direct and reflected radiation as represented by the first and second term of (5). Close to the emitter the ratio Π/Π_{pr} is obviously unity, but soon we reach the distance where it can be said that the interference maxima lie on the curve C_1 given by $|\Pi/\Pi_{pr}|=1+\alpha_{11}|R_{11}|$ and the minima on the curve C_2, viz. $|\Pi/\Pi_{pr}|=1-\alpha_{11}|R_{11}|$. It is seen from fig. 2 that the distance $2\alpha_{11}|R_{11}|$ between C_1 and C_2 shows a minimum at D=0·4 km., this being due to the Brewster minimum in the reflexion. It may be remarked that beyond this minimum the effect of the divergence factor α_{11} becomes more and more of importance; if we had wrongly considered the reflexion to take place against a flat earth, the interference minimum at D=13 km., *e. g.*, would have become 0·066 instead of 0·096.

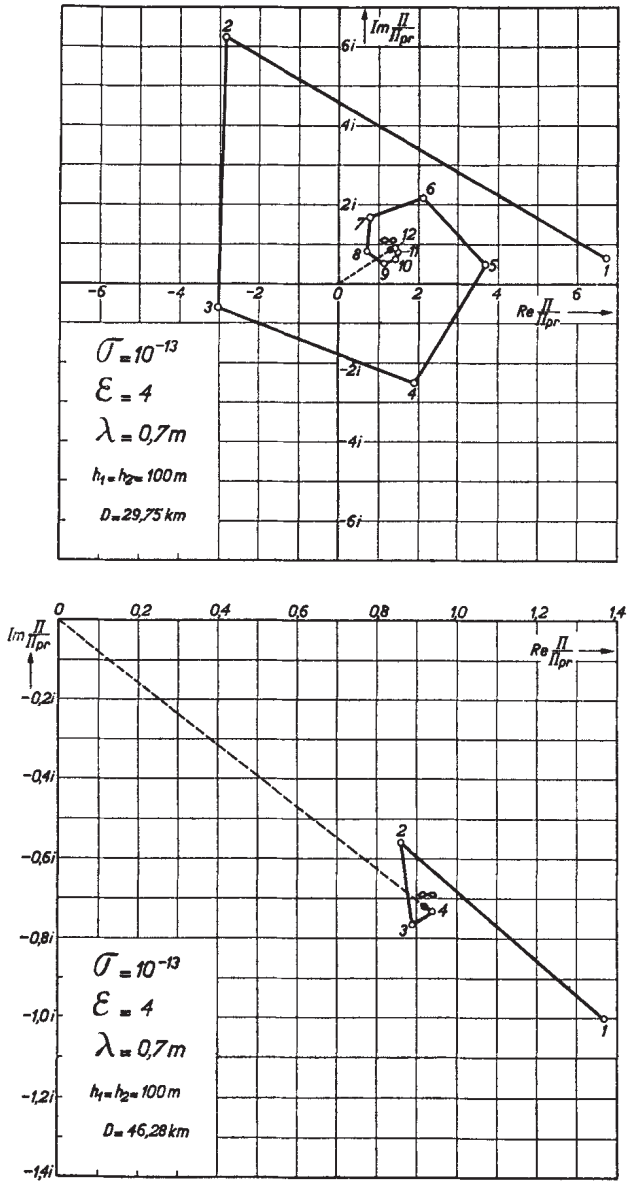
When we approach the shadow limit and penetrate into it the residue series formula (4 *b*) must be used. Therefore in fig. 2 all the points calculated from the geometric-optical formula (5) are shown as black circles, whereas those obtained from the residue series as open circles. The numbers placed near these open circles represent the number of terms of the residue series which were necessary in order to obtain an accuracy of one per cent. The figure shows very clearly how this number

Fig. 2.



An example (λ=70 cm.) showing the interference phenomena in the lit region and the transition from the geometric-optical results (5) shown as ● to those obtained from the residue series (4 *b*) shown as ○.

Fig. 3.

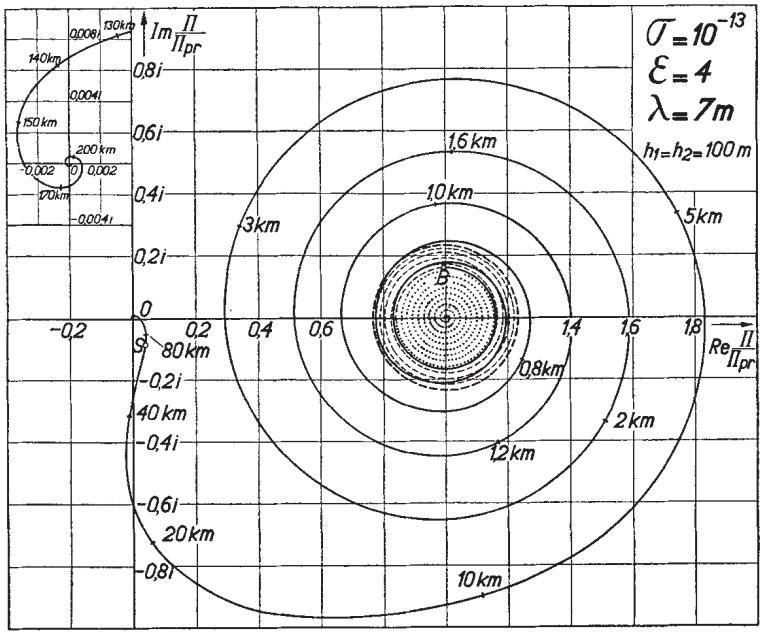


Two examples showing the evaluation of the residue series as a vectorial addition of its successive terms. The top drawing refers to a point between the last interference maximum and minimum, whereas the lower figure refers to a point between the last maximum and the shadow limit.

of terms rapidly increases from one well beyond the shadow limit, up to 10 to 17 near the first interference maximum. Moreover, it demonstrates the excellent fit obtained in the overlapping range which occurs near this first interference maximum.

Turning next to fig. 3 we there represent for two special cases the vectorial addition of the several complex terms of the residue series, viz., for $\sigma=10^{-13}$, $\epsilon=4$, $\lambda=0{\cdot}7$ m., $h_1=h_2=100$ m., and the distances D=29·75 and 46·28 km. The numbers placed near the corners of the broken spirals indicate the summation of 1, 2, ... terms of the series.

Fig. 4.



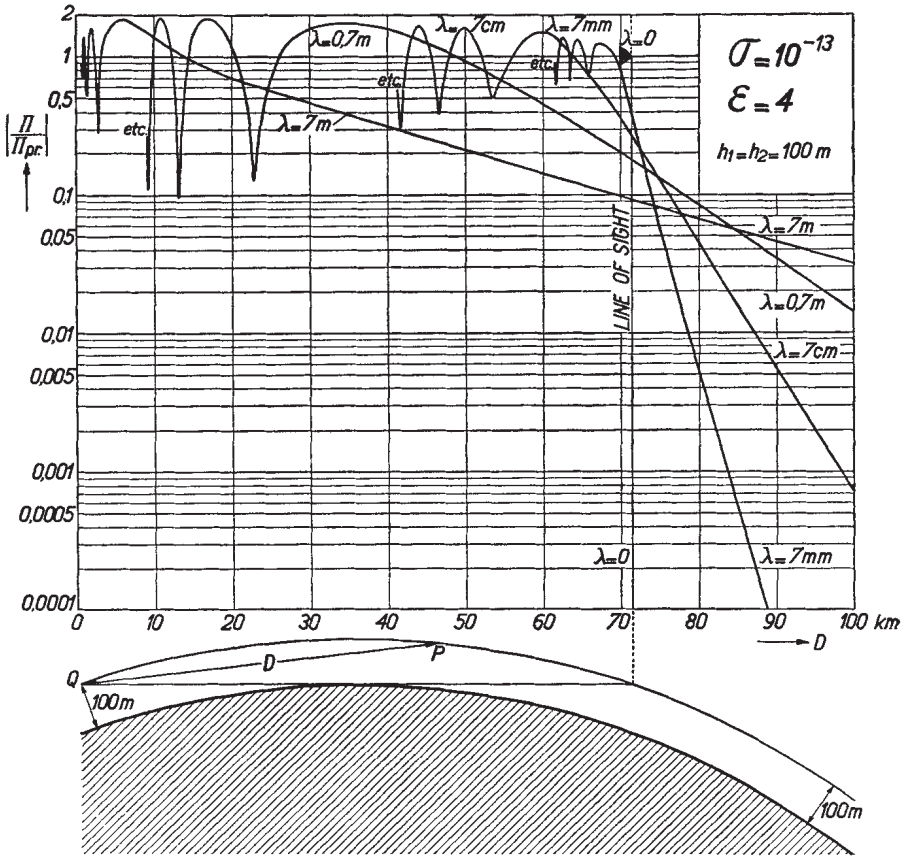
An example showing what becomes of the Cornu spiral of optics for the diffraction of radio waves round an absorbing sphere.

In order to obtain with sufficient accuracy the final vector, indicated by the dotted line from the origin, thirteen terms were necessary in the top curve, whereas only four terms were sufficient in the case of the lower figure, which refers to a bigger distance.

Coming next to the rather complicated fig. 4, which was calculated for $\sigma=10^{-13}$, $\epsilon=4$, $\lambda=7$ m., $h_1=h_2=100$ m., this drawing represents what becomes of the well-known Cornu spiral in our special diffraction problem with absorption. The numbers 3 km., 5 km., 10 km..... etc. placed near the curve indicate the distance of the receiver from the emitter,

and the vector drawn from the origin O to any point on the spiral represents, both in amplitude and phase, the ratio of the actual field at the corresponding distance to the field which would obtain there in the absence of the diffracting earth. If we follow the spiral from the centre $(1+oi)$, which corresponds to the receiver near the emitter, it first spirals out and

Fig. 5.

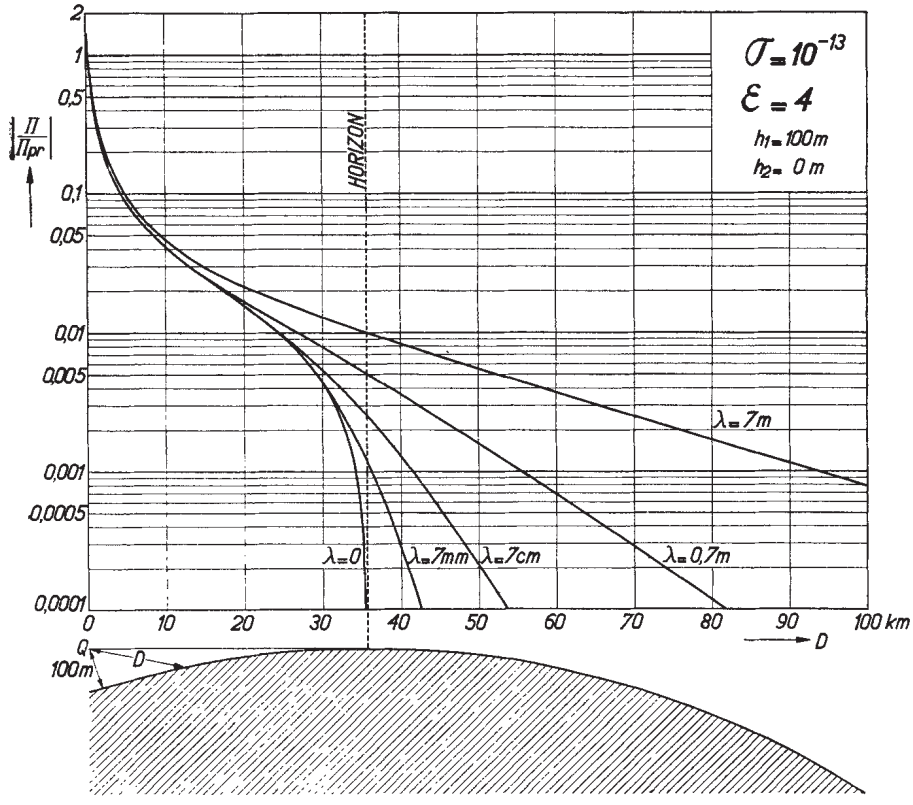


The attenuation factor for short waves when both emitter and receiver are at a height of 100 m. and for propagation over average soil.

then shrinks again to a minimum value at (B) corresponding to the Brewster minimum, as fully explained with fig. 2 ; next it expands again (the radius corresponding all the time to $\alpha_{11} \mid R_{11} \mid$) till it bends over at the point S, where the shadow limit is reached, finally to approach the origin O again in a spiral way, but with inversed rotation, the details of this latter part being given in the left top drawing.

Having thus explained some details of our general numerical procedure we give in figs. 5 and 6 the final results. Both figures have again been calculated for $\sigma=10^{-13}$, $\epsilon=4$, $\lambda=7$ m., 0·7 m., 7 cm., and 7 mm. Fig. 5 relates to the case where both emitter and receiver are at 100 metres height ($h_1=h_2=100$ m.), whereas in fig. 6 the emitter is supposed at $h_1=100$ metres, the receiver being on the ground ($h_2=0$), where it may be remarked that, due to the principle of reciprocity, the last figure also

Fig. 6.



The attenuation factor for short waves of the field at the surface of the earth when the emitter is at a height of 100 m. and for propagation over average soil.

refers to the case where the emitter and receiver are interchanged. Thus the present more accurate fig. 5 has to replace fig. 20 of II. and the present fig. 6, fig. 19 of II. Fig. 5 clearly shows again that a wave $\lambda=7$ metres penetrates well into the optical shadow region, no discontinuity whatever occurring at the shadow limit. As found before, only waves of a length

of the order of one centimetre or shorter exhibit a rapid cut-off when we pass into this shadow region.

The general behaviour of the curves of fig. 5 can be described as follows :—The final decrease for short waves starts already at the last interference maxima (the one nearest the shadow limit), the slope of the curve varying further only very little when we enter into the shadow region. It should be observed that this last maximum occurs the nearer the shadow limit the shorter the wave-length, it lying *on* this limit when $\lambda \to 0$, for which case an infinite sharp cut-off occurs.

Turning now to fig. 6, this has been drawn for the same constants of the earth and wave-lengths, only $h_1 = 100$ m. and $h_2 = 0$. Here obviously no interference maxima and minima occur, the curves being of a fully monotonic character with a complete absence again of any discontinuity at the horizon. Before the horizon the geometric-optical formula (5) was again used up to the transition region, after which the residue series (4 *b*) was applied. Moreover, in this case, where the receiver is on the ground, we have for all distances two simplifications in the general formula (5), viz., $\alpha_{11} = 1$, and $D = R_1 + R_2$.

It is further seen that before the horizon the curves asymptotically approach the limiting curve for $\lambda \to 0$, which latter case could be very simply treated with the aid of (5), because then the conduction current is negligible compared with the dielectric displacement current ($k_2^2 \to \epsilon\omega^2/c^2$), leading quite simply to

$$\frac{\Pi}{\Pi_{pr}} = \frac{2\epsilon \cos \tau_2}{\epsilon \cos \tau_2 + \sqrt{\epsilon - \sin^2 \tau_2}},$$

where τ_2 is the angle of incidence of the direct ray at the receiving point.

In conclusion, the feeling may be expressed that, as far as we are aware, the new curves given here, and which are again based on the hypothesis of a homogeneous atmosphere, constitute the most accurate and detailed theoretical results so far published because they were derived with one single approximation to the Bessel functions, viz., what we have called the *Hankel* approximation.

Eindhoven.
31st October, 1938.